Chapter 1

Nuclear Fusion I

> *"Fusion powers the stars: light nuclei climb the binding curve toward iron, releasing energy, if they can tunnel the Coulomb barrier."*
>
> standard astrophysical summary [6, 14]

Fission exploits the decline of B/A for heavy nuclei. Fusion exploits the *rise* of B/A for light nuclei. This chapter reads the binding-energy curve as a map of energy release, derives the fusion Q-value from binding energies with a neon–neon example, introduces the sharp-surface contact estimate $V_{\text{contact}} = Z_1 Z_2 e^2/[4\pi\varepsilon_0(r_1 + r_2)]$, evaluates its scale for $\text{Ne} + \text{Ne}$ and $p + p$, and explains why stellar fusion proceeds by quantum tunneling at thermal energies far below the barrier [6, 1, 14, 2].

1.1 The binding-energy curve: fission right, fusion left

Figure 1.1 summarises nuclear energetics. The label "most stable" in the original slide should be read as "near the maximum of B/A": among measured nuclides ^{62}Ni has the largest binding energy per nucleon, whereas ^{56}Fe is especially abundant and is commonly used to mark the end of exothermic stellar burning.

- B/A rises steeply from the lightest nuclei toward $A \sim 56$–62 (the Fe–Ni region).
- After the peak, B/A decreases slowly through the heavy elements.

Any nuclear rearrangement that increases the total binding energy decreases the rest mass and releases energy $Q = (\Delta M)c^2$.

Fission (right of the peak). A heavy parent ($A \sim 240$, $B/A \sim 7.6\,\text{MeV}$) splits into medium-mass fragments nearer the peak ($B/A \sim 8.5\,\text{MeV}$). Energy is released; this was the subject of Lectures 23–24.

Fusion (left of the peak). Two light nuclei combine into a heavier product still left of or nearer the peak. The product has larger B/A than the reactants, so energy is released. The classic laboratory example is

$$\text{D} + \text{T} \;\to\; ^{4}\text{He} + n + 17.6\,\text{MeV}, \tag{1.1}$$

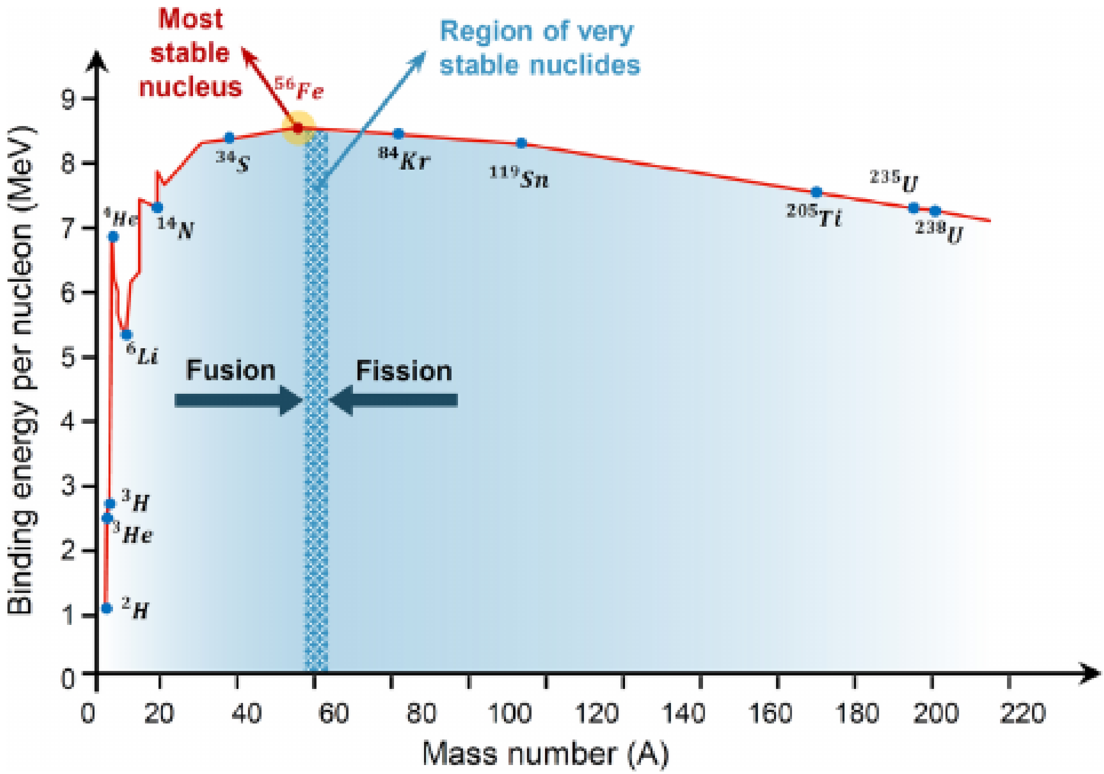

Figure 1.1: Binding energy per nucleon B/A versus mass number A, cleanly cropped from the original Lecture 26 figure. The peak near iron/nickel marks the most tightly bound nuclei. Fusion of light nuclei (left of the peak) and fission of heavy nuclei (right of the peak) both move systems toward higher B/A and release energy. Re-extracted from PH5001 lecture material (Prof. Bharat Kumar).

and in stars the pp chain begins with $p + p \to \mathrm{d} + e^+ + \nu_e$.

Key idea

Fusion: light nuclei join and move up the B/A curve toward iron. Fission: heavy nuclei split and move up the B/A curve from the other side. Both release energy; both are blocked by barriers (Coulomb for fusion, deformation for fission).

Beyond the Fe–Ni peak, charged-particle fusion generally ceases to be a steady energy source. Most nuclei heavier than iron are assembled instead by slow or rapid neutron capture followed by β^- decays; explosive environments can also drive selected endothermic charged-particle and photodisintegration sequences. Thus "fusion stops at iron" is a statement about stellar energy generation, not a claim that heavier nuclei cannot be synthesized [1, 2].

1.2 Fusion Q-value from binding energies

For a general fusion reaction

$$X + Y \to Z + \cdots, \tag{1.2}$$

the Q-value is

$$Q = [M_X + M_Y - M_Z - \cdots]c^2. \tag{1.3}$$

Writing each mass as $Mc^2 = \sum m_N c^2 - E_B$ and cancelling free nucleon masses (when nucleon number is conserved) yields the binding form

$$Q = E_B(\text{final}) - E_B(\text{initial}). \tag{1.4}$$

Fusion releases energy when the product is more tightly bound than the sum of the reactants: $E_B(\text{final}) > E_B(\text{initial})$.

1.2.1 Binding bookkeeping for the radiative neon channel

Consider

$${}^{20}_{10}\mathrm{Ne} + {}^{20}_{10}\mathrm{Ne} \;\to\; {}^{40}_{20}\mathrm{Ca} + \gamma. \tag{1.5}$$

(This is a valid radiative-capture channel for binding-energy bookkeeping, but it is not representative of the dominant decay of the highly excited ${}^{40}\mathrm{Ca}^*$ compound system.)

Rest energy before fusion. One neon nucleus has rest energy

$$E({}^{20}\mathrm{Ne}) = (10m_p + 10m_n)c^2 - E_B({}^{20}\mathrm{Ne}). \tag{1.6}$$

Two neon nuclei contribute

$$E_{\text{before}} = 2(10m_p + 10m_n)c^2 - 2E_B({}^{20}\mathrm{Ne}). \tag{1.7}$$

Rest energy after fusion.

$$E(^{40}\text{Ca}) = (20m_p + 20m_n)c^2 - E_B(^{40}\text{Ca}). \tag{1.8}$$

Q-value.

$$\begin{aligned} Q &= E_{\text{before}} - E_{\text{after}} \\ &= 2(10m_p + 10m_n)c^2 - 2E_B(\text{Ne}) - \left[(20m_p + 20m_n)c^2 - E_B(\text{Ca})\right] \\ &= E_B(^{40}\text{Ca}) - 2E_B(^{20}\text{Ne}). \end{aligned} \tag{1.9}$$

Equivalently, in terms of binding per nucleon,

$$Q = 40\left[\left(\frac{B}{A}\right)_{\text{Ca}} - \left(\frac{B}{A}\right)_{\text{Ne}}\right]. \tag{1.10}$$

Since $(B/A)_{\text{Ca}} > (B/A)_{\text{Ne}}$ on the rising part of the curve, $Q > 0$. The raw lecture estimated $Q \simeq 23\,\text{MeV}$ from a schematic B/A graph. Evaluated atomic masses give a more accurate result. Because both sides contain 20 electrons when neutral-atom masses are used, electron masses cancel:

$$\begin{aligned} Q &= \left[2M_{\text{a}}(^{20}\text{Ne}) - M_{\text{a}}(^{40}\text{Ca})\right] c^2 \\ &= [2(19.992\,440\,1762) - 39.962\,590\,863]\,\text{u}\,c^2 \\ &= 0.022\,289\,4894\,\text{u}\,c^2 = 20.76\,\text{MeV}, \end{aligned} \tag{1.11}$$

where $1\,\text{u}\,c^2 = 931.494\,\text{MeV}$. Thus the original binding-energy logic is sound, but its graph-read value is about $2.2\,\text{MeV}$ too large. For the idealized radiative-capture channel in Eq. (1.5), the energy ultimately appears in the photon and calcium recoil [27, 6].

At neon-burning energies the compound nucleus has open particle channels. Representative measured two-body exit channels include

$$^{20}\text{Ne} + {}^{20}\text{Ne} \to {}^{36}\text{Ar} + \alpha, \tag{1.12}$$

$$^{20}\text{Ne} + {}^{20}\text{Ne} \to {}^{39}\text{K} + p. \tag{1.13}$$

Additional multi-particle channels occur as energy increases. Their Q-values must be computed from the masses of the actual final products; the $20.76\,\text{MeV}$ value above belongs only to the radiative $^{40}\text{Ca} + \gamma$ channel [27, 1].

Remark

Equation (1.4) is the same identity used for fission ($Q = E_{B,\text{frag}} - E_{B,\text{parent}}$). Only the direction of motion on the B/A curve changes.

1.3 The Coulomb barrier

Although fusion of light nuclei is energetically favoured, the nuclei are positively charged. They repel until they approach within the range of the attractive nuclear force ($\sim$ a few fm). The electrostatic potential energy at centre-to-centre separation r is

$$V_C(r) = \frac{Z_1 Z_2 e^2}{4\pi\varepsilon_0\, r}. \tag{1.14}$$

As r decreases, V_C rises. When the nuclear surfaces touch, the nuclear attraction rapidly dominates and the potential drops into a deep well. The value of V_C at contact provides a useful sharp-surface estimate:

$$\boxed{V_{\text{contact}} = \frac{Z_1 Z_2 e^2}{4\pi\varepsilon_0\,(r_1 + r_2)}.} \tag{1.15}$$

The actual barrier V_B is the maximum of the combined Coulomb, nuclear, and centrifugal effective potential; it depends on diffuse nuclear density profiles, angular momentum, and the adopted ion–ion potential.

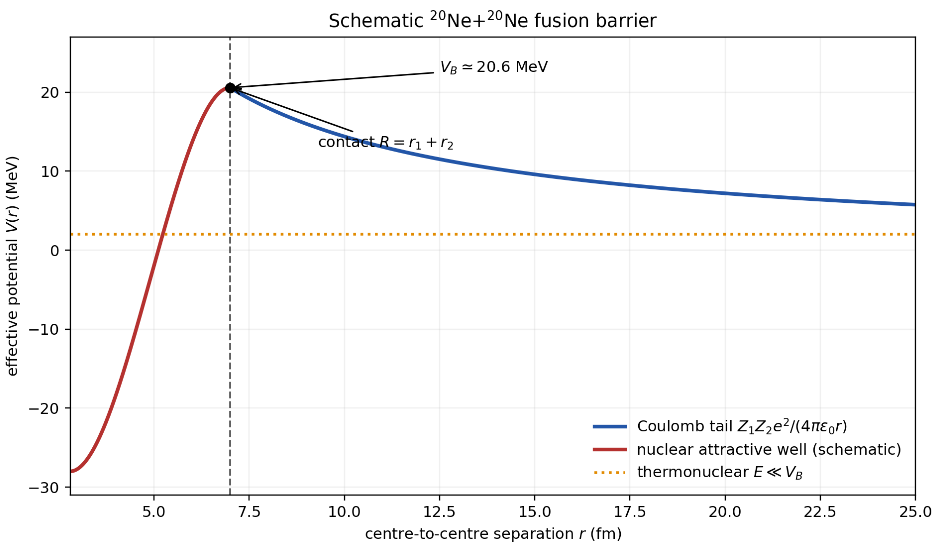

Figure 1.2: Schematic effective potential for $^{20}\text{Ne} + {}^{20}\text{Ne}$. The Coulomb tail rises toward the contact radius, while the short-range nuclear attraction produces an interior well. The contact estimate is $V_{\text{contact}} \simeq 20.6\,\text{MeV}$; a quantitative barrier requires an ion–ion potential and partial-wave specification.

Nuclear radii follow the empirical law

$$r = r_0 A^{1/3}, \qquad r_0 \approx 1.2\,\text{fm}. \tag{1.16}$$

A convenient numerical constant is

$$\frac{e^2}{4\pi\varepsilon_0} \approx 1.44\,\text{MeV}\cdot\text{fm}, \tag{1.17}$$

so

$$V_{\text{contact}} \approx \frac{Z_1 Z_2 \times 1.44\,\text{MeV}\cdot\text{fm}}{r_1 + r_2}. \tag{1.18}$$

1.3.1 Example: neon–neon

For two ^{20}Ne nuclei, $Z_1 = Z_2 = 10$, $A = 20$:

$$r_1 = r_2 = 1.2 \times 20^{1/3}\,\text{fm} \approx 1.2 \times 2.71\,\text{fm} \approx 3.26\text{–}3.5\,\text{fm} \tag{1.19}$$

(using the lecture's 3.5 fm estimate). Contact separation $r_1 + r_2 \approx 7.0\,\text{fm}$, so

$$V_{\text{contact}} = \frac{10 \times 10 \times 1.44\,\text{MeV} \cdot \text{fm}}{7.0\,\text{fm}} \approx 20.6\,\text{MeV} \sim 20\,\text{MeV}. \tag{1.20}$$

Classically one needs $\sim 20\,\text{MeV}$ of relative kinetic energy to surmount the barrier.

1.3.2 Example: proton–proton

For $p + p$, $Z_1 = Z_2 = 1$. If one adopts the conventional pedagogical contact scale $R = 2\,\text{fm}$,

$$V_{\text{contact}} = \frac{1 \times 1 \times 1.44\,\text{MeV} \cdot \text{fm}}{2\,\text{fm}} = 0.72\,\text{MeV}. \tag{1.21}$$

The proton has no sharp classical surface, so 0.72 MeV is a contact-scale estimate rather than a uniquely defined barrier height; changing the chosen strong-interaction radius changes this number. It nevertheless shows that the Coulomb scale is huge compared with thermal energies in the solar core (Section 1.4) [6, 1, 14, 2].

Key idea

$V_{\text{contact}} = Z_1 Z_2 e^2/[4\pi\varepsilon_0(r_1 + r_2)]$, $r = r_0 A^{1/3}$. Ne + Ne: $V_{\text{contact}} \sim 20\,\text{MeV}$. $p + p$: $V_{\text{contact}} \sim 0.72\,\text{MeV}$, subject to the chosen contact radius. The Coulomb scale grows rapidly with $Z_1 Z_2$.

1.4 Classical threshold vs quantum tunneling

1.4.1 Classical requirement

Classically, fusion requires relative kinetic energy

$$E_k > V_B, \qquad V_B \sim V_{\text{contact}} = \frac{Z_1 Z_2 e^2}{4\pi\varepsilon_0(r_1 + r_2)} \tag{1.22}$$

in the sharp-surface estimate. Accelerators can supply tens of MeV and drive fusion reactions for nuclear physics studies, but the energy invested in the beams typically exceeds the energy recovered from Q: accelerators are not practical power plants.

1.4.2 Quantum tunneling and reduced mass

Separate the two-body motion into centre-of-mass and relative coordinates. The relative coordinate behaves as one particle of reduced mass

$$\mu = \frac{m_1 m_2}{m_1 + m_2}, \qquad E = \frac{1}{2}\mu v^2, \qquad v = |\boldsymbol{v}_1 - \boldsymbol{v}_2|. \tag{1.23}$$

For $E < V_{\max}$, WKB gives

$$P(E) \simeq \exp\left[-2\int_R^{r_c} \frac{\sqrt{2\mu[V_C(r)-E]}}{\hbar}\,dr\right], \qquad r_c = \frac{K}{E}, \quad K = \frac{Z_1 Z_2 e^2}{4\pi\varepsilon_0}, \tag{1.24}$$

where $R \simeq r_1 + r_2$ and r_c are the inner and outer turning points. At thermonuclear energies $R/r_c \ll 1$. With $r = r_c \sin^2\theta$, the leading Coulomb integral is

$$\begin{aligned} 2\int_0^{r_c} \frac{\sqrt{2\mu(K/r-E)}}{\hbar}\,dr &= \frac{4Er_c}{\hbar}\sqrt{\frac{2\mu}{E}}\int_0^{\pi/2}\cos^2\theta\,d\theta \\ &= \frac{\pi K}{\hbar}\sqrt{\frac{2\mu}{E}} = \frac{2\pi K}{\hbar v} \equiv 2\pi\eta, \end{aligned} \tag{1.25}$$

because $\int_0^{\pi/2}\cos^2\theta\,d\theta = \pi/4$. The Sommerfeld parameter and Gamow energy are therefore

$$\eta = \frac{K}{\hbar v} = Z_1 Z_2 \alpha\frac{c}{v}, \qquad P(E) \propto e^{-2\pi\eta} = \exp\left[-\sqrt{\frac{E_G}{E}}\right], \qquad E_G = 2\mu c^2(\pi\alpha Z_1 Z_2)^2. \tag{1.26}$$

Finite-R and nuclear-structure effects are later absorbed into the measured cross section and astrophysical S-factor. Since $2\pi\eta \propto 1/v \propto E^{-1/2}$, penetration rises exponentially with energy. This is the same physics as α decay (Lectures 16–17), run in reverse: instead of tunneling *out*, the nuclei tunnel *in* [6, 14].

1.4.3 Thermonuclear fusion

In a hot plasma the kinetic energy is thermal. The mean kinetic energy of a particle is

$$\langle E_k\rangle = \frac{3}{2}k_B T. \tag{1.27}$$

Fusion powered by the thermal motion of a plasma is called **thermonuclear fusion**. It is the energy source of main-sequence stars and the goal of magnetic and inertial confinement fusion devices.

Room temperature. At $T \approx 300\,\mathrm{K}$,

$$k_B T \approx 0.026\,\mathrm{eV}, \tag{1.28}$$

utterly negligible compared with even the *pp* barrier of 720 keV. The tunneling probability is zero for practical purposes.

Temperature for $E_k \sim 150\,\mathrm{keV}$. Set $\frac{3}{2}k_B T = 150\,\mathrm{keV}$, so $k_B T = 100\,\mathrm{keV}$:

$$T = \frac{100\times 10^3\,\mathrm{eV}}{8.617\times 10^{-5}\,\mathrm{eV/K}} \approx 1.16\times 10^9\,\mathrm{K}. \tag{1.29}$$

This calculation only asks what temperature would make the *mean* single-particle energy 150 keV; it is not an ignition condition. Practical D–T plasmas use $k_B T$ of order 10 keV and still rely on tunneling.

Solar core. The Sun's core has $T \approx 1.5 \times 10^7\,\mathrm{K}$, so

$$k_B T \approx 1.3\,\mathrm{keV}, \qquad \langle E_k \rangle \sim 2\,\mathrm{keV} \tag{1.30}$$

(order 1 keV in the lecture's estimate). Thus $V_{\max}/k_B T \approx 720/1.3 \approx 550$. Fusion in the Sun is possible only because of tunneling, aided by two further facts:

(i) the Maxwell–Boltzmann distribution has a high-energy tail, so some protons have $E \gg \langle E_k \rangle$;

(ii) the solar core is extremely dense ($\rho \sim 150\,\mathrm{g\,cm^{-3}}$) and huge, so even a tiny rate per pair yields enormous luminosity.

Caution

Do not equate $k_B T$ with the barrier height. Stars and fusion reactors operate with $k_B T \ll V_{\max}$; the Gamow tunneling factor and the Maxwell tail jointly set the rate (Lecture 26).

1.4.4 Salpeter plasma screening

The Coulomb field in a plasma is weakly screened by surrounding electrons and ions. In the Debye–Hückel limit the screening cloud lowers the free-energy cost of bringing charges $Z_1 e$ and $Z_2 e$ together. Salpeter's weak-screening result multiplies the unscreened thermonuclear rate by

$$f_{\mathrm{sc}} = \exp\left(\frac{Z_1 Z_2 e^2}{4\pi\varepsilon_0 R_D k_B T}\right) > 1, \qquad R_D^{-2} = \frac{e^2}{\varepsilon_0 k_B T} \sum_s n_s Z_s^2. \tag{1.31}$$

This is a modest rate enhancement under solar-core conditions, not removal of the Coulomb barrier. Its validity requires weak screening; that condition is stated explicitly in Lecture 26 [36].

1.5 Maxwell tail and barrier penetration

In a gas at temperature T the speed distribution is Maxwellian. A fraction of particles has kinetic energy many times $k_B T$:

$$E \sim 10\,k_B T,\ 20\,k_B T,\ \dots \tag{1.32}$$

Those particles tunnel far more readily because $2\pi\eta \propto 1/v \propto 1/\sqrt{E}$. The fusion rate is therefore dominated by a compromise between the falling Maxwell factor $e^{-E/k_B T}$ and the rising penetration factor $e^{-b/\sqrt{E}}$. The product peaks at the **Gamow peak**, derived properly in the next chapter.

The barrier penetration probability for energy E may be written as a WKB integral between classical turning points r_1 and r_2:

$$P \sim \exp\left(-2\int_{r_1}^{r_2} \sqrt{\frac{2\mu}{\hbar^2}\left(V(r) - E\right)}\,\mathrm{d}r\right), \tag{1.33}$$

with $V(r) = Z_1 Z_2 e^2/(4\pi\varepsilon_0 r)$ outside the nuclear well. Increasing E shrinks the integration range and the integrand, so P grows rapidly with energy [6, 14, 2].

1.6 Reaction rate preview

The number of fusion reactions per unit volume per unit time between species X and Y is

$$r_{XY} = \frac{n_X n_Y}{1+\delta_{XY}}\,\langle\sigma v\rangle, \tag{1.34}$$

where n_X, n_Y are number densities, σ is the fusion cross section, v is the relative velocity, and $\langle\sigma v\rangle$ is the thermal average. The Kronecker delta supplies 1/2 for identical reactants, so each unordered pair is counted once. The energy generation rate is $r_{XY}Q$ per unit volume. Concentrations and temperature therefore control stellar luminosity and the performance of fusion devices. The full derivation of R from beam–target geometry, the $1/v^2$ low-energy cross section, and the S-factor form of the low-energy cross section, and the Gamow peak occupies Lecture 26.

Takeaway

- B/A peaks at Fe/Ni: fusion left of peak, fission right of peak.
- $Q = E_B(\text{final}) - E_B(\text{initial})$; for $\text{Ne}+\text{Ne} \to \text{Ca}$, $Q = E_B(\text{Ca}) - 2E_B(\text{Ne}) = 20.76\,\text{MeV}$.
- The sharp-surface contact estimate is $V_{\text{contact}} = Z_1 Z_2 e^2/[4\pi\varepsilon_0(r_1+r_2)]$; $\text{Ne}+\text{Ne} \sim 20\,\text{MeV}$, while the quoted $pp \sim 0.72\,\text{MeV}$ depends on the chosen contact radius.
- Thermonuclear fusion: $E \sim k_B T \ll V_{\max}$; tunneling $P \propto e^{-2\pi\eta}$; solar core $T \sim 1.5\times10^7\,\text{K}$, $E \sim 1\,\text{keV}$.
- Salpeter weak screening multiplies the unscreened rate by $f_{\text{sc}} > 1$ in a weakly coupled plasma.
- Rate $r_{XY} = n_X n_Y\langle\sigma v\rangle/(1+\delta_{XY})$ (derived next).

1.7 Deeper physics: Coulomb barrier and sub-barrier tunneling

1.7.1 Contact Coulomb barrier

For two nuclei of charges $Z_1 e$ and $Z_2 e$ and radii $R_i = r_0 A_i^{1/3}$, the Coulomb potential at contact is

$$V_{\text{C}}(R_1+R_2) = \frac{Z_1 Z_2 e^2}{4\pi\varepsilon_0(R_1+R_2)}. \tag{1.35}$$

This sets the scale of the fusion barrier height $V_{\max}$ in a one-dimensional model [6, 14]. Because $V_{\text{C}} \propto Z_1 Z_2/A^{1/3}$, heavier-projectile combinations face higher barriers and require higher centre-of-mass energy for appreciable fusion [1, 53].

Barrier heights for light and heavy fusion

For $^{12}\mathrm{C} +^{12}\mathrm{C}$ with $R_1 + R_2 \approx 5.2\,\mathrm{fm}$ and $Z_1 Z_2 = 144$, $V_{\max} \approx 2.5\,\mathrm{MeV}$ [6, 14]. For $^{48}\mathrm{Ca} +^{248}\mathrm{Cm}$ ($Z_1 Z_2 = 4800$, $R_1 + R_2 \approx 12\,\mathrm{fm}$), $V_{\max} \approx 30\,\mathrm{MeV}$ [53]. Stellar burning never reaches these heavy-ion barriers in equilibrium; superheavy synthesis relies on sub-barrier tunneling and evaporation-residue survival.

1.7.2 Sub-barrier tunneling

Classically, fusion requires $E_{\mathrm{CM}} \geq V_{\max}$. Quantum mechanically, the colliding nuclei tunnel through the barrier. The Gamow penetration factor for fusion mirrors α decay (Lectures 16–17) with incoming rather than outgoing boundary conditions:

$$P \approx \exp\left[-\frac{2}{\hbar}\int_R^b \sqrt{2\mu(V(r)-E)}\,\mathrm{d}r\right]. \tag{1.36}$$

At energies well below $V_{\max}$, P rises steeply with E. Deformed targets and transfer channels can enhance sub-barrier fusion beyond the s-wave estimate, while quasifission removes flux before evaporation [53, 14]. Terrestrial D–T reactors operate at $T \sim 10^8\,\mathrm{K}$ where the Maxwellian tail supplies enough $E > V_{\max}$ events, supplemented by tunneling (Lecture 26) [1, 2].

Key idea

Assumptions of the one-dimensional barrier model. The sketch neglects angular momentum (centrifugal barrier), nuclear absorption, and compound-nucleus lifetime. It remains the correct first estimate for why fusion rates are exponentially sensitive to $Z_1 Z_2$ and why the Sun burns hydrogen slowly enough to shine for gigayears [36, 6].

1.7.3 The S-factor connection to Lecture 26

Laboratory fusion data are reported as $S(E) = E\,\sigma(E)\exp(\sqrt{E_G/E})$, removing the steep Gamow energy dependence [14, 36]. The same WKB exponent that appears in α decay (Lectures 16–17) defines $E_G = 2\mu(\pi\alpha Z_1 Z_2 \hbar c)^2$. Sub-barrier heavy-ion fusion cross sections are therefore the incoming-channel counterpart of α-decay rates, with $S(E)$ playing the role of a nuclear structure factor analogous to the preformation factor S_α [6, 53]. Stellar rates integrate $S(E)$ over the Maxwellian Gamow peak (Lecture 26).

1.7.4 Lawson criterion and ignition temperature

Terrestrial fusion must exceed losses as well as penetrate the Coulomb barrier. A crude Lawson criterion requires the product of density n and energy confinement time τ_E to exceed a threshold that depends on temperature and fuel cycle [1, 6]. For D–T, $\langle\sigma v\rangle$ peaks near $T \sim 10^8\,\mathrm{K}$; for $p + p$ in the Sun, the peak is at much lower T but the weak pp step limits the overall burn rate (Lecture 26) [36, 14]. Magnetic and inertial confinement schemes both operate in the sub-barrier tunneling regime rather than at $E = V_{\max}$ [2, 1].

Coupled-channel barrier distributions replace a single barrier height with a weighted set of eigenbarriers. Measuring fusion excitation functions below the nominal barrier therefore constrains deformation and transfer couplings. For SHE, the evaporation-residue cross section folds fusion probability with survival against fission: both pieces are uncertain.

1.8 Further physics from the literature

Sequence and scope. The presentation follows the pedagogical order used in H. C. Verma's nuclear physics series: fusion energetics and the Coulomb barrier; thermonuclear reactors; then stellar fusion, neutrinos, and stellar nucleosynthesis. The two PH5001 source lectures are reorganized across Chapters 25–26 in that order, with reaction-rate calculus placed between the barrier and applications [32].

Stellar versus terrestrial fusion. A star confines plasma gravitationally for millions to billions of years and can obtain useful luminosity from extraordinarily slow reactions. In particular, $p + p \to d + e^+ + \nu_e$ requires the weak interaction, which makes the Sun stable on gigayear scales. A terrestrial device has a much smaller fuel inventory and confinement time, so it chooses the much faster strong reaction D–T, heats the plasma externally, and must recover energy while replacing radiative, transport, and particle losses. "Lowest Coulomb barrier" alone therefore does not determine the fuel: nuclear matrix elements, resonances, density, and confinement matter as well.

Stellar burning stages. Hydrogen burning (*pp* chain and CNO cycle) dominates main-sequence stars. When core hydrogen is exhausted, contraction raises T until helium burning ($3\alpha \to {}^{12}\mathrm{C}$) ignites, then carbon, neon, oxygen, and silicon burning in massive stars, ending at the iron peak where fusion no longer releases energy [14, 6, 2].

Screening and plasma effects. The derivation uses bare nuclei. In a plasma, correlations among electrons and ions lower the free-energy cost of bringing two reacting ions together. In weak screening the rate is multiplied by an enhancement $f_{\mathrm{sc}} > 1$; one should not describe this as simply replacing the Coulomb potential by a constant lower barrier over all radii. Laboratory targets also have bound electrons and require a distinct electron-screening correction before their data are extrapolated to a stellar plasma [14, 36].

Laboratory fusion approaches. Magnetic confinement (tokamaks, stellarators) and inertial confinement (laser or ion-beam driven pellets) both aim for thermonuclear $\mathrm{D} + \mathrm{T}$ conditions. Neither is required to reach $E = V_{\max}$; both rely on tunneling at $T \sim 10^8\,\mathrm{K}$ [1, 2].

Connection to α decay. The Gamow factor for fusion is the time-reversed cousin of the Gamow factor for α emission (Lectures 16–17). The same WKB integral appears with incoming versus outgoing boundary conditions [6, 14].

Reading guide

Krane [6] (fusion overview and barriers); Dunlap [1] (energetics); Basdevant [14] (stellar fusion and S-factors); Demtröder [2] (experimental and astrophysical context).

1.8.1 Sub-barrier fusion cross section scaling

Below the Coulomb barrier, the fusion cross section is dominated by tunneling. A useful parameterisation writes

$$\sigma(E) \approx \frac{S(E)}{E} \exp(-2\pi\eta(E)), \qquad \eta(E) = \frac{Z_1 Z_2 e^2}{4\pi\varepsilon_0 \hbar v}, \tag{1.37}$$

where η is the Sommerfeld parameter [14, 6]. As $E \to 0$, $\eta \to \infty$ and $\sigma \to 0$ exponentially. Coupled-channel calculations show that static deformation can enhance $\sigma(E)$ by an order of magnitude at fixed E because the effective barrier is lowered along the orientation that aligns the major axis [53].

Sub-barrier $^{12}\mathrm{C} + ^{12}\mathrm{C}$ fusion

At $E_{\mathrm{CM}} = 2\,\mathrm{MeV}$, well below $V_{\max} \approx 2.5\,\mathrm{MeV}$, measured fusion cross sections are $\sim 10^{-4}\,\mathrm{mb}$, many orders of magnitude below $\sigma_{\mathrm{geom}} \approx 850\,\mathrm{mb}$ [6, 14]. The same Gamow exponent that gives $t_{1/2} \sim 10^{-7}\,\mathrm{s}$ for $^{212}\mathrm{Po}$ α decay (Lecture 17) governs this incoming channel. Stellar $^{12}\mathrm{C}$ burning occurs at temperatures where the Gamow peak sits near $E_0 \sim 1.5\,\mathrm{MeV}$ (Lecture 26) [36].

1.8.2 From Coulomb barriers to stellar Gamow peak

Terrestrial magnetic confinement operates at $T \sim 10^8\,\mathrm{K}$ where $k_B T \approx 10\,\mathrm{keV}$, comparable to D–T barrier penetration energies. Stellar cores at $T \sim 1.5 \times 10^7\,\mathrm{K}$ have $k_B T \approx 1.3\,\mathrm{keV}$, far below the $p + p$ barrier, yet burn steadily because $\langle \sigma v \rangle$ integrates over a Maxwellian tail [36, 2]. Screening in the plasma enhances rates by $\exp(U_e/k_B T)$ with $U_e \sim 1$–$2\,\mathrm{keV}$ at solar density [14, 36]. The lecture barrier estimate is therefore a zero-screening baseline.

Remark

Quasifission in heavy-ion fusion removes flux before compound-nucleus formation, analogous to hindrance factors suppressing α decay without changing the barrier integral. SHE synthesis cross sections are limited by both tunneling and survival against fission (Lecture 23) [53, 54].

1.8.3 Terrestrial D–T versus stellar *pp* burning

Terrestrial fusion targets D–T because $\langle \sigma v \rangle$ peaks near $T \sim 10^8\,\mathrm{K}$ with a manageable confinement requirement [1, 6]. The solar *pp* chain relies on the same tunneling physics at $T \sim 1.5 \times 10^7\,\mathrm{K}$ where the weak $p + p$ step sets the overall timescale (Lecture 26) [36, 14]. The Coulomb barrier for $p + p$ is lower than for D–T, but the weak interaction makes *pp* enormously slower than D–T at comparable temperature. This contrast explains why stars are stable for gigayears while fusion devices require external heating and choose the fastest exothermic strong-interaction channel available [2, 36].

1.8.4 Electron screening in laboratory versus stellar plasmas

Laboratory fusion experiments on solid targets require electron-screening corrections before extrapolating to bare-nucleus astrophysical rates [36, 14]. In stellar plasmas, weak Debye screening enhances rates by $f_{\mathrm{sc}} \approx \exp(U_e/k_B T)$ without replacing the Coulomb barrier by a constant lower value at all radii [36]. The lecture contact-barrier estimate is the zero-screening baseline; Solar Fusion III curates recommended S-factors together with screening uncertainties for each light-ion channel [36, 6]. Sub-barrier heavy-ion fusion for SHE synthesis adds coupled-channel and quasifission complications beyond either screening correction [53, 54].

1.9 Deeper reading: Coulomb barriers, coupled channels, and SHE

The contact Coulomb barrier $Z_1 Z_2 e^2/(4\pi\varepsilon_0(R_1 + R_2))$ sets the scale for light-ion fusion and for heavy-ion synthesis. Sub-barrier fusion is enhanced or suppressed by deformation and transfer channels in coupled-channel models. Quasifission can remove flux before a compound nucleus forms, which is why SHE cross sections are not simple tunneling estimates.

Stellar fusion of light nuclei (Lecture 26) uses the same barrier physics at much lower energies, packaged as S-factors. Estimate barriers for $^{12}\mathrm{C} + {}^{12}\mathrm{C}$ and for a $^{48}\mathrm{Ca}$-induced SHE reaction to feel the gap between astrophysics and superheavy programmes.

Barrier distributions

Experimental fusion barrier distributions are extracted from derivatives of excitation functions. Peaks correspond to couplings to rotational or vibrational channels. Comparing a spherical projectile on a deformed target versus the reverse kinematics tests the coupling picture.

Survival probability

Forming a compound nucleus is not enough: it must survive fission to reach the ground state by neutron evaporation. Shell-stabilised residues have higher survival. That competition, not the Coulomb barrier alone, limits SHE synthesis rates.

Barrier comparison

Estimate contact barriers for pp, $^{12}\mathrm{C} + {}^{12}\mathrm{C}$, and $^{48}\mathrm{Ca} + {}^{248}\mathrm{Cm}$. The progression from kilo-electronvolt stellar scales (after tunneling) to hundreds of mega-electronvolts for SHE entrance channels shows why astrophysics and superheavy synthesis share formulas but not facilities.

Discuss one coupled-channel effect qualitatively: a deformed target presents a lower barrier at the tips, enhancing sub-barrier fusion. Then note quasifission as a competing dynamical process that can still suppress residue formation. Lecture 26 next packages the light-ion end of this physics into stellar rates; SHE research lives at the opposite extreme of the same tunneling idea.

Fusion tunneling unifies stellar burning and superheavy synthesis. Coupled channels and quasifission decide how far simple barrier estimates can be trusted.

In practice, rework one numerical estimate from the lecture with a different parameter set and compare the shift to the quoted experimental uncertainty. If the shift exceeds the uncertainty, the estimate is teaching a scale, not delivering a fit. That distinction keeps theoretical cartoons honest when they sit beside evaluated data tables and modern many-body calculations. Along the course arc, write one sentence linking this chapter backward and one forward: the discipline of those two sentences is as important as any single formula. Examination problems rarely ask for a literature review, but they do ask for the scale argument that literature reviews presuppose.

Synthesis problem

Write a half-page note that (i) restates the chapter's central scale or selection rule in one equation, (ii) evaluates it numerically for one concrete nucleus or energy, and (iii) names the neighbouring lecture that uses the result. Keep the note free of research-frontier speculation; the goal is fluency with the lecture physics itself. If an assumption fails (Born approximation, spherical mean field, allowed transition, one-dimensional barrier), state the failure mode in a final sentence. That habit converts passive reading into examination-ready understanding and makes the later research-frontier box read as an extension rather than a replacement.

Research frontier: sub-barrier fusion and superheavy synthesis

Coulomb-barrier tunneling (Lecture 25) governs both stellar burning and heavy-ion fusion used to synthesise superheavy elements. Coupled-channel models show that deformation and transfer channels can enhance or suppress sub-barrier fusion relative to a single-barrier estimate [53]. Synthesis of elements beyond oganesson requires new projectile–target combinations and higher beam intensities; theory and experiment remain tightly coupled [52]. For light systems, recommended astrophysical S-factors are curated in Solar Fusion III, providing a complementary low-energy application of the same tunneling physics [36]. Uncertainties that still limit SHE programmes include fusion-evaporation survival probabilities, the role of quasifission, and incomplete knowledge of optimal excitation energies. The lecture's barrier-penetration estimate is the right starting point before those coupled-channel and dynamical complications are added.

In SHE synthesis, the competition between fusion and quasifission means that a larger geometric overlap does not automatically yield more evaporation residues. Coupled-channel enhancement at sub-barrier energies can be offset by dynamical breakup of the composite system. That tension is the modern reading of the lecture tunneling estimate.

Quasifission can erase a coupled-channel fusion gain, which is why SHE cross sections remain hard to predict from barrier height alone.

Proposal writing for new SHE reactions therefore mixes tunneling estimates with dynamical transport simulations.

Student directions. (1) Barrier estimate: compute the contact Coulomb barrier for ${}^{12}\mathrm{C}+{}^{12}\mathrm{C}$ and for ${}^{48}\mathrm{Ca}+{}^{248}\mathrm{Cm}$. (2) Qualitative reasoning: explain why a deformed target can increase the sub-barrier fusion probability. (3) Literature status: summarise attempts to synthesise $Z = 119$ or 120 from a recent review [53].

1.10 Problems with solutions

Problem 25.1 — Q from B/A for $\mathrm{D}+\mathrm{T}$

The reaction $\mathrm{D}+\mathrm{T} \to {}^4\mathrm{He}+n$ has $Q = 17.6\,\mathrm{MeV}$. If the total binding energy of $\mathrm{D}+\mathrm{T}$ is B_i and that of ${}^4\mathrm{He}$ is $B_\alpha = 28.3\,\mathrm{MeV}$ (the neutron is unbound as a free particle, $B_n = 0$), find B_i from $Q = B_f - B_i$ and comment [6, 1].

Solution 25.1

Step 1. Final binding: $B_f = B_\alpha + B_n = 28.3\,\mathrm{MeV}$.
Step 2.

$$Q = B_f - B_i \quad \Rightarrow \quad B_i = B_f - Q = 28.3 - 17.6 = 10.7\,\mathrm{MeV}.$$

That matches $B(\mathrm{d}) + B(\mathrm{t}) \approx 2.2 + 8.5 = 10.7\,\mathrm{MeV}$. Fusion increases total binding by $17.6\,\mathrm{MeV}$.

Problem 25.2 — Neon fusion Q structure

Starting from rest energies expressed with binding energies, derive $Q = E_B({}^{40}\mathrm{Ca}) - 2E_B({}^{20}\mathrm{Ne})$ for ${}^{20}\mathrm{Ne} + {}^{20}\mathrm{Ne} \to {}^{40}\mathrm{Ca} + \gamma$. Then use $M_a({}^{20}\mathrm{Ne}) = 19.992\,440\,1762\,\mathrm{u}$, $M_a({}^{40}\mathrm{Ca}) = 39.962\,590\,863\,\mathrm{u}$, and $1\,\mathrm{u}c^2 = 931.494\,\mathrm{MeV}$ to check the lecture's graph-read estimate.

Solution 25.2

Step 1. Follow Eqs. (1.7)–(1.9): nucleon mass terms cancel, leaving $Q = E_B(\mathrm{Ca}) - 2E_B(\mathrm{Ne})$.
Step 2. Atomic masses may be used directly because 20 atomic electrons occur on each side:

$$\Delta M = 2(19.992\,440\,1762) - 39.962\,590\,863 = 0.022\,289\,4894\,\mathrm{u}.$$

Step 3.

$$Q = \Delta M c^2 = (0.022\,289\,4894)(931.494) = 20.76\,\mathrm{MeV}.$$

The corresponding exact difference in binding per nucleon is $Q/40 = 0.519\,\mathrm{MeV}$, not the schematic $0.58\,\mathrm{MeV}$. The original derivation is correct; only its low-resolution graph estimate needed correction [27].

Problem 25.3 — Coulomb barrier for ${}^{12}\mathrm{C} + {}^{12}\mathrm{C}$

Estimate $V_{\max}$ for two ${}^{12}\mathrm{C}$ nuclei. Use $r = 1.2\,A^{1/3}\,\mathrm{fm}$ and $e^2/(4\pi\varepsilon_0) = 1.44\,\mathrm{MeV}\cdot\mathrm{fm}$.

Solution 25.3

Step 1.

$$r = 1.2 \times 12^{1/3} = 1.2 \times 2.29 \approx 2.75\,\mathrm{fm}, \qquad r_1 + r_2 = 5.50\,\mathrm{fm}.$$

Step 2.

$$V_{\text{max}} = \frac{6 \times 6 \times 1.44}{5.50} = \frac{51.84}{5.50} \approx 9.4\,\text{MeV}.$$

Carbon burning in massive stars must tunnel a $\sim 10\,\text{MeV}$ barrier [6, 14].

Problem 25.4 — *pp* contact scale and solar k_BT

Show that $V_{\text{contact}}(pp) \approx 0.72\,\text{MeV}$ if the pedagogical contact radius is chosen as $r_1 + r_2 = 2\,\text{fm}$. At $T = 1.5 \times 10^7\,\text{K}$, compute k_BT in keV and the ratio V_{contact}/k_BT.

Solution 25.4

Step 1.

$$V_{\text{contact}} = \frac{1.44\,\text{MeV} \cdot \text{fm}}{2\,\text{fm}} = 0.72\,\text{MeV}.$$

Step 2.

$$k_BT = (8.617 \times 10^{-5}\,\text{eV/K}) \times 1.5 \times 10^7\,\text{K} \approx 1.29 \times 10^3\,\text{eV} \approx 1.3\,\text{keV}.$$

Step 3.

$$\frac{V_{\text{contact}}}{k_BT} = \frac{720\,\text{keV}}{1.3\,\text{keV}} \approx 550.$$

The proton has no sharp classical surface, so this is a radius-dependent Coulomb scale, not a uniquely measured barrier. Its enormous ratio to k_BT still demonstrates why solar fusion requires tunneling [6, 2].

Problem 25.5 — Temperature for $150\,\text{keV}$

What temperature T gives $\frac{3}{2}k_BT = 150\,\text{keV}$? Compare with the solar core temperature.

Solution 25.5

$$k_BT = 100\,\text{keV}, \qquad T = \frac{100 \times 10^3}{8.617 \times 10^{-5}} \approx 1.16 \times 10^9\,\text{K}.$$

This is about 80 times hotter than the solar core ($\sim 1.5 \times 10^7\,\text{K}$). Laboratory fusion concepts operate near 10^8 K with tunneling still essential [1, 14].

Problem 25.6 — Fusion vs fission energy per nucleon

Compare Q/A for (a) fission with $Q = 200\,\text{MeV}$, $A = 236$; (b) D + T fusion with $Q = 17.6\,\text{MeV}$ and 5 nucleons in the reactants. Which releases more energy per nucleon?

Solution 25.6

(a)

$$\frac{Q}{A} = \frac{200}{236} \approx 0.85\,\text{MeV/nucleon}.$$

(b)

$$\frac{Q}{A} = \frac{17.6}{5} = 3.52\,\text{MeV/nucleon}.$$

Fusion of light nuclei releases several times more energy *per nucleon* than fission, which is why fusion fuels are attractive despite the barrier challenge [6, 1].

Bibliography

[1] R. A. Dunlap, *An Introduction to the Physics of Nuclei and Particles* (2nd ed.), IOP Publishing, Bristol (2023), DOI: 10.1088/978-0-7503-6094-4, Ch. 3 (Nuclear composition and size).

[2] W. Demtröder, *Nuclear and Particle Physics*, Undergraduate Lecture Notes in Physics, Springer, Cham (2023).

[3] S. Petrera, *Problems and Solutions in Nuclear and Particle Physics*, UNITEXT for Physics, Springer, Cham (2019).

[4] F. Terranova, *A Modern Primer in Particle and Nuclear Physics*, Oxford University Press (2021).

[5] S. D'Auria, *Introduction to Nuclear and Particle Physics*, Undergraduate Lecture Notes in Physics, Springer, Cham (2018).

[6] K. S. Krane, *Introductory Nuclear Physics*, Wiley, New York (1988).

[7] R. Hofstadter, "Electron scattering and nuclear structure," Rev. Mod. Phys. **28**, 214 (1956).

[8] H. F. Ehrenberg, R. Hofstadter, U. Meyer-Berkhout, D. G. Ravenhall, and S. E. Sobottka, "High-Energy Electron Scattering and the Charge Distribution of Carbon-12 and Oxygen-16," Phys. Rev. **113**, 666 (1959).

[9] H. Yukawa, "On the interaction of elementary particles. I," Proc. Phys.-Math. Soc. Japan **17**, 48 (1935).

[10] R. D. Woods and D. S. Saxon, "Diffuse surface optical model for nucleon-nuclei scattering," Phys. Rev. **95**, 577 (1954).

[11] H. G. J. Moseley, "The high-frequency spectra of the elements," Phil. Mag. **26**, 1024 (1913); **27**, 703 (1914).

[12] C. F. von Weizsäcker, "Zur Theorie der Kernmassen," Z. Phys. **96**, 431 (1935).

[13] P. Cappellaro, *Introduction to Applied Nuclear Physics* (MIT OpenCourseWare / LibreTexts), CC BY-NC-SA 4.0.

[14] J.-L. Basdevant, J. Rich, and M. Spiro, *Fundamentals in Nuclear Physics: From Nuclear Structure to Cosmology*, Springer, New York (2005).

[15] D. Tong, *Particle Physics*, Lecture notes (University of Cambridge / CERN school notes).

[16] M. G. Mayer, "On closed shells in nuclei. II," Phys. Rev. **75**, 1969 (1949).

[17] O. Haxel, J. H. D. Jensen, and H. E. Suess, "On the "magic numbers" in nuclear structure," Phys. Rev. **75**, 1766 (1949).

[18] T. Schmidt, "Über die magnetischen Momente der Atomkerne," Z. Phys. **106**, 358 (1937).

[19] L. W. Nordheim, "On spins, moments, and shells in nuclei," Phys. Rev. **78**, 294 (1950).

[20] Evaluated Nuclear Structure Data File (ENSDF), National Nuclear Data Center, Brookhaven National Laboratory, `https://www.nndc.bnl.gov/ensdf/`.

[21] NuDat 3, National Nuclear Data Center, Brookhaven National Laboratory, `https://www.nndc.bnl.gov/nudat3/`.

[22] N. J. Stone, "Table of nuclear magnetic dipole and electric quadrupole moments," At. Data Nucl. Data Tables **90**, 75 (2005); updated compilations at NNDC.

[23] W. N. Cottingham and D. A. Greenwood, *An Introduction to Nuclear Physics* (2nd ed.), Cambridge University Press, Cambridge (2001).

[24] H. Geiger and J. M. Nuttall, "The ranges of the α particles from the radioactive substances," Phil. Mag. **22**, 613 (1911).

[25] G. Gamow, "Zur Quantentheorie des Atomkernes," Z. Phys. **51**, 204 (1928).

[26] R. W. Gurney and E. U. Condon, "Wave mechanics and radioactive disintegration," Nature **122**, 439 (1928); Phys. Rev. **33**, 127 (1929).

[27] M. Wang, W. J. Huang, F. G. Kondev, G. Audi, and S. Naimi, "The AME 2020 atomic mass evaluation (II). Tables, graphs and references," Chin. Phys. C **45**, 030003 (2021).

[28] Laboratoire National Henri Becquerel (LNHB), Recommended decay data, `http://www.lnhb.fr/nuclear-data/nuclear-data-table/`.

[29] L. M. Langer, R. D. Moffat, and H. C. Price, Jr., "Low energy beta-ray spectra: P^{32} and Cu^{64}," Phys. Rev. **76**, 1725 (1949).

[30] L. M. Langer and H. C. Price, Jr., "Shapes of the beta-spectra of the forbidden transitions of Sb^{124}, Rb^{86}, Sr^{89}, Y^{91}, and Cs^{137}," Phys. Rev. **75**, 1769 (1949).

[31] D. C. Camp and L. M. Langer, "The shape of the ^{66}Ga positron spectrum and the contribution from $0^+ \to 0^+$ transitions," Phys. Rev. **129**, 1782 (1963).

[32] H. C. Verma, *Nuclear Physics: Fundamentals and Applications*, NPTEL/IIT Kanpur lecture series, `https://hcverma.in/ncl_phy_lectures`.

[33] International Atomic Energy Agency, *LiveChart of Nuclides*, evaluated structure, decay, reaction, and fission-yield data, `https://www-nds.iaea.org/relnsd/vcharthtml/VChartHTML.html`.

[34] T. Kibédi, T. W. Burrows, M. B. Trzhaskovskaya, P. M. Davidson, and C. W. Nestor, Jr., "Evaluation of theoretical conversion coefficients using BrIcc," Nucl. Instrum. Methods Phys. Res. A **589**, 202 (2008), DOI: 10.1016/j.nima.2008.02.051.

[35] D. A. Brown *et al.*, "ENDF/B-VIII.0: The 8th major release of the nuclear reaction data library with CIELO-project cross sections, new standards and thermal scattering data," Nucl. Data Sheets **148**, 1 (2018), DOI: 10.1016/j.nds.2018.02.001.

[36] B. Acharya *et al.*, "Solar fusion III: New data and theory for hydrogen-burning stars," Rev. Mod. Phys. **97**, 035002 (2025), DOI: 10.1103/8lm7-gs18.

[37] S. N. Ghoshal, "An experimental verification of the theory of compound nucleus," Phys. Rev. **80**, 939 (1950), DOI: 10.1103/PhysRev.80.939.

[38] D. Adhikari *et al.* (PREX Collaboration), "Accurate determination of the neutron skin thickness of ^{208}Pb through parity-violation in electron scattering," Phys. Rev. Lett. **126**, 172502 (2021), DOI: 10.1103/PhysRevLett.126.172502.

[39] B. T. Reed, F. J. Fattoyev, C. J. Horowitz, and J. Piekarewicz, "Implications of PREX-II on the equation of state of neutron-rich matter," Phys. Rev. Lett. **126**, 172503 (2021), DOI: 10.1103/PhysRevLett.126.172503.

[40] B. Hu *et al.*, "Ab initio predictions link the neutron skin of ^{208}Pb to nuclear forces," Nature Phys. **18**, 1196 (2022), DOI: 10.1038/s41567-022-01715-8.

[41] E. Epelbaum, H.-W. Hammer, and U.-G. Meißner, "Modern theory of nuclear forces," Rev. Mod. Phys. **81**, 1773 (2009), DOI: 10.1103/RevModPhys.81.1773.

[42] H.-W. Hammer, S. König, and U. van Kolck, "Nuclear effective field theory: Status and perspectives," Rev. Mod. Phys. **92**, 025004 (2020), DOI: 10.1103/RevModPhys.92.025004.

[43] T. Otsuka, A. Gade, O. Sorlin, T. Suzuki, and Y. Utsuno, "Evolution of shell structure in exotic nuclei," Rev. Mod. Phys. **92**, 015002 (2020), DOI: 10.1103/RevModPhys.92.015002.

[44] H. Hergert, S. K. Bogner, T. D. Morris, A. Schwenk, and K. Tsukiyama, "The in-medium similarity renormalization group: A novel ab initio method for nuclei," Phys. Rep. **621**, 165 (2016), DOI: 10.1016/j.physrep.2015.12.007.

[45] J. M. Lattimer and M. Prakash, "The equation of state of hot, dense matter and neutron stars," Phys. Rep. **621**, 127 (2016), DOI: 10.1016/j.physrep.2015.12.005.

[46] J. M. Lattimer, "Neutron stars and the nuclear matter equation of state," Annu. Rev. Nucl. Part. Sci. **71**, 433 (2021), DOI: 10.1146/annurev-nucl-102419-124827.

[47] B. P. Abbott *et al.* (LIGO Scientific Collaboration and Virgo Collaboration), "GW170817: Observation of gravitational waves from a binary neutron star inspiral," Phys. Rev. Lett. **119**, 161101 (2017), DOI: 10.1103/PhysRevLett.119.161101.

[48] M. J. Dolinski, A. W. P. Poon, and W. Rodejohann, "Neutrinoless double-beta decay: Status and prospects," Annu. Rev. Nucl. Part. Sci. **69**, 219 (2019), DOI: 10.1146/annurev-nucl-101918-023407.

[49] M. Agostini, G. Benato, J. A. Detwiler, J. Menéndez, and F. Vissani, "Toward the discovery of matter creation with neutrinoless $\beta\beta$ decay," Rev. Mod. Phys. **95**, 025002 (2023), DOI: 10.1103/RevModPhys.95.025002.

[50] P. Gysbers *et al.*, "Discrepancy between experimental and theoretical β-decay rates resolved from first principles," Nature Phys. **15**, 428 (2019), DOI: 10.1038/s41567-019-0450-7.

[51] H. L. Crawford, K. Fossez, S. König, and A. Spyrou, "A vision for the science of rare isotopes," Annu. Rev. Nucl. Part. Sci. **74**, 141 (2024), DOI: 10.1146/annurev-nucl-121423-091501.

[52] Nuclear Science Advisory Committee, *A New Era of Discovery: The 2023 Long Range Plan for Nuclear Science*, U.S. Department of Energy and National Science Foundation (2023), `https://nuclearsciencefuture.org/`.

[53] S. A. Giuliani, Z. Matheson, W. Nazarewicz, E. Olsen, P.-G. Reinhard, J. Sadhukhan, B. Schuetrumpf, N. Schunck, and P. Schwerdtfeger, "Colloquium: Superheavy elements: Oganesson and beyond," Rev. Mod. Phys. **91**, 011001 (2019), DOI: 10.1103/RevModPhys.91.011001.

[54] N. Schunck and D. Regnier, "Theory of nuclear fission," Prog. Part. Nucl. Phys. **125**, 103963 (2022), DOI: 10.1016/j.ppnp.2022.103963.

[55] I. Counts, J. Hur, D. P. L. Aude Craik, H. Jeon, C. Leung, J. C. Berengut, A. Geddes, A. Kawasaki, W. Jhe, and V. Vuletić, "Evidence for nonlinear isotope shift in Yb^+ search for new boson," Phys. Rev. Lett. **125**, 123002 (2020), DOI: 10.1103/PhysRevLett.125.123002.

[56] I. Angeli and K. P. Marinova, "Table of experimental nuclear ground state charge radii: An update," At. Data Nucl. Data Tables **99**, 69 (2013), DOI: 10.1016/j.adt.2011.12.006.

[57] S. Kraemer *et al.*, "Observation of the radiative decay of the ^{229}Th nuclear clock isomer," Nature **617**, 706 (2023), DOI: 10.1038/s41586-023-05894-z.